Direct coupling of a high temperature proton exchange membrane fuel cell with hydrogen produced by catalytic partial dehydrogenation of a gasoline-ethanol blend (E10)

Rafael Garcia Garrido, Mélanie Taillades-Jacquin, Gilles Taillades, Frédéric Lecoeur, Nicolas Donzel, Marc Dupont, Julian Dailly, Marion Scohy, Jacques Rozière, Deborah J Jones

Direct coupling of a high temperature proton exchange membrane fuel cell with hydrogen produced by catalytic partial dehydrogenation of a gasoline-ethanol blend (E10)

Rafael Garcia Garrido[a], Mélanie Taillades-Jacquin[a,], Gilles Taillades[a], Frédéric Lecoeur[a], Nicolas Donzel[a], Marc Dupont[a], Julian Dailly[b], Marion Scohy[c], Jacques Rozière[a], Deborah J. Jones[a]*

[a]Institut Charles Gerhardt UMR 5253, Agrégats, Interfaces et Matériaux pour l'Energie, Université de Montpellier, CNRS, ENSCM, Place Eugène Bataillon, 34095 Montpellier Cedex 5, France
[b]European Institute for Energy Research, Emmy-Noether-Str. 11, 76131 Karlsruhe, Germany
[c]Safran Power Units, 8 Chemin du Pont de Rupé, 31200 Toulouse, France

(*) corresponding author: melanie.taillades-jacquin@umontpellier.fr

Keywords

Fuels; Gasoline E10; Partial dehydrogenation; Hydrogen generation; High temperature proton exchange membrane fuel cell; Liquid organic hydrogen carrier; Pt-Sn-In; alumina

Abstract

The on-board partial dehydrogenation of gasoline to generate hydrogen of sufficient purity to feed a fuel cell directly requires catalysts producing high purity hydrogen at high rate, while also preserving the defining density and boiling point properties of gasoline to allow its recycle to the fuel tank. Here, hydrogen of purity >98 % is produced by the catalytic partial dehydrogenation of gasoline SP95E10 (containing 10 % ethanol) with a productivity of 2300 $NL \cdot h^{-1} \cdot kg_{cat}^{-1}$ using a Pt-Sn-In/alumina catalyst prepared by templating and incipient wetness impregnation. The hydrogen is used to feed a high temperature proton exchange membrane fuel cell. The difference in performance between the fuel cell fed with pure hydrogen and with hydrogen generated from gasoline reaches only 13 mV at 200 $mA \cdot cm^{-2}$ at 160 °C, and the loss is completely recovered when the anode gas stream is reverted to pure hydrogen. Such reversible performance loss is attributable to the presence of carbon monoxide that is formed from oxygenated hydrocarbons during the partial dehydrogenation reaction. The depleted gasoline retains its physical properties and presents significantly lower sulfur content, opening prospects for power generation on-board a vehicle with a fuel cell using hydrogen produced on demand from its primary fuel.

1. Introduction

Hydrogen as an energy carrier has a clean energy cycle, high energy efficiency and it can be produced by diverse processes [1]. Furthermore, it is a renewable energy carrier and it can be used in fuel cells with no point-of-use emissions [2,3]. However, one of the most important challenges for the viable use of hydrogen concerns its storage and distribution, taking into account its low density in the gaseous state and the fact that its volumetric energy density is $1/10^{th}$ that of gasoline [4]. Exhaust gas assisted reforming of gasoline or diesel fuel with steam on-board a vehicle generates hydrogen as a replacement for a fraction of the liquid fuel in gasoline engines to improve engine efficiency and emissions performance [5,6]. Steam reforming of diesel or kerosene fuels or their surrogates to produce syngas to feed a solid oxide fuel cell for on-board auxiliary power units [7], or a gas stream of sufficiently low carbon monoxide content for a high temperature proton exchange membrane fuel cell have been reported [8,9], but no experimental results of the coupling between the hydrogen generation and hydrogen conversion steps were described. Nevertheless, the study of methanol steam reforming coupled with high temperature fuel cells for on-board application has shown promising results [10–13]. Partial oxidation of ethanol/gasoline blends is an alternative method for hydrogen and carbon monoxide production for mobile power generation in solid oxide fuel cells [14]. Liquid organic hydrogen carriers store hydrogen by reversible hydrogenation of a carrier material unsaturated hydrocarbons [15,16]. Partial dehydrogenation (PDh) of hydrocarbons enables production of highly pure hydrogen and is applicable in principle to any transport fuel, including kerosene, diesel and gasoline [16–23]. On-board hydrogen generation is possible, thereby avoiding high-pressure hydrogen storage or the use of cryogenic tanks. Pt/Al_2O_3 catalysts are commonly used for hydrogenation-dehydrogenation, oxidations and reforming reactions [24,25]. Platinum-functionalised catalysts have a high affinity to break the C-H bond, while the affinity to break the

C-C bond is low, decreasing the cracking reaction and increasing the selectivity for dehydrogenation reactions [26]. The addition of tin to Pt/Al_2O_3 improves the performance and the stability of the catalyst for alkane dehydrogenation [23,26–30], and indium found to reduce the amount of coke formed in the proximity of platinum particles, serving to stabilise the catalyst activity [31]. In previous work, we and others have studied the partial dehydrogenation of Jet A-1 fuel, low sulfur (3 ppm sulfur) Jet A-1 [23], kerosene [22], gasoline and diesel surrogate fuels [17] using alumina supported platinum-tin and indium-doped $Pt\text{-}Sn/Al_2O_3$ [7], as well as nickel and cobalt phosphides supported on Cab-o-sil [32]. E10 is a petrol blend containing up to 10% renewable ethanol. E10 leads to lower carbon dioxide emissions and higher octane rating than non-blended gasoline, and the trend in its use in Europe is increasing, being boosted by European biofuels targets for transport fuels, as well as in the USA [33]. Super Premier 95 E10 (95 octane) is a mixture of hydrocarbons and eventually oxygenated organic compounds with up to 10 vol.% ethanol, and with the following compositional specifications: aromatics ≤ 35 vol.%; olefins ≤ 18 vol.%; benzene ≤ 1 vol.%; oxygen ≤ 10 vol.%; ethyl tert-butyl ether ≤ 22 vol.%; Mn ≤ 2 $mg \cdot L^{-1}$; Pb ≤ 5 $mg \cdot L^{-1}$; S ≤ 10 $mg \cdot kg^{-1}$; zero phosphorus containing compounds, as well as anticorrosion additives and stabilisers [34]. Because of the presence of oxygen-containing organic compounds, partial dehydrogenation of E10 gasoline is expected to lead to a hydrogen gas stream containing carbon monoxide as a conversion product, and the hydrogen produced is therefore more suitable to feed a high temperature proton exchange membrane fuel cell (HT-PEMFC) where the tolerance to CO at 160-200 °C is 2-3 % [35]. Water and oxygenate impurities in the liquid organic hydrogen carrier perhydro dibenzyltoluene (H18-DBT) were also reported to be a source of carbon monoxide on dehydrogenation, highlighting the need for drying and pre-purification of H18-DBT [36]. Gasoline E10 also contains up to 10 ppm of sulfur that could generate H_2S [37]

or other volatile sulfur containing molecules, as well as nitrogen-containing compounds, that are also potential poisons for the fuel cell catalyst.

We have investigated the catalytic partial dehydrogenation of E10 gasoline at reaction temperatures of 370 and 400 °C using an In-Pt-Sn/Al_2O_3 catalyst, and studied the stability of the catalyst with time on stream as well as the composition of the gas produced. The purity of the hydrogen, greatly improved by implementing a cold trap to remove light hydrocarbons, was sufficiently high to be used directly in a high temperature PEMFC without further purification; and we describe below how the performance of the HT-PEMFC was affected by irreversible and reversible losses directly related to the feed gas composition.

2. Experimental

2.1 Fuel

The fuel used for the catalytic partial dehydrogenation is a commercial unleaded gasoline containing up to 10% of bio-sourced ethanol, SP95E10, the characteristics of which are provided in Table S1.

2.2 Catalyst preparation

The Pt-Sn-In/Al_2O_3 (Pt=1 wt.%, Sn=1 wt.% and In=0,5 wt.%) was prepared by incipient wetness impregnation following our previous work [17]. The alumina support was prepared by the sol-gel method using $AlCl_3 \cdot 6H_2O$ (Alfa Aesar), sucrose as porogen (Alfa Aesar), NH_4OH for regulation of the pH and deionized water. The synthesis was performed with a mole ratio of 1:0.5:75 of Al:sucrose:H_2O. $AlCl_3 \cdot 6H_2O$ was dissolved in water, the sucrose was added and the pH was adjusted to 5 while stirring at 200 rpm. The gel that formed was stirred for 5 h, and then heated at 80 °C until dry. It was calcined at 600 ºC for 6 h in a static oven with air extraction,

leading to a white powder of aluminum oxide. Impregnation was performed into the alumina support in two steps, first an aqueous solution of $InCl_3$ (Acros) was used to impregnate the alumina support to give 0.5 wt.% and then it was dried at 80 ºC overnight. A second impregnation was carried out using an aqueous solution prepared by adding $SnCl_2 \cdot 2H_2O$ (Acros) dissolved in 1 M HCl to a solution of $H_2PtCl_6 \cdot 6H_2O$ (Alfa Aesar) to give a ratio of 1 wt.% Pt and 1 wt.% Sn. After impregnation the catalyst was dried at 80 ºC overnight and thermally treated in an oven with air extraction at 120 ºC for 2 h and then at 560 ºC for 2 h with a ramp rate of 2 $^{\circ}C \cdot min^{-1}$.

2.3 Catalyst characterization

X-Ray diffraction (XRD) analyses for structural investigation of the samples were performed using a PANalytical X'Pert diffractometer, with CuK_α radiation (λ=0.15418 nm, 40 kV, 25 mA) using an acquisition time of 60 minutes. HighScore software by PANalytical was used to identify the compounds present.

Scanning electron microscopy (SEM) was performed with an electronic microscope Hitachi S-2600N equipped with an Oxford Instrument X-Max 80 mm^2 for energy dispersive X-ray spectroscopy (EDS).

Nitrogen adsorption measurements were performed on 3Flex-3500 volumetric analyzer from Micromeritics equipped with 10 and 0.1 Torr pressure transducers. Before adsorption experiments the samples were degassed under vacuum (0.001 Torr) for 12 h at 473 K. Isotherm data were collected at 77 K in the range of relative pressure [10^{-9}-1]. The specific surface area was calculated using the Brunauer–Emmett–Teller method (BET) within the relative pressure range of 0.05-0.3. Pore size distributions were calculated using Barrett - Joyner - Halenda method

(BJH) using the Micromeritics implemented software (3Flex version 5.0); pore volume values are related to the condensation point at $P/P^0 = 0.99$.

NH_3 temperature programmed desorption (NH_3-TPD) for the measure of surface acidity of the materials was studied with an Autochem 2910 automatic system from Micromeritics. Samples were heated to 550 ºC in a helium flow of 30 ml·min^{-1} (heating rate 5 °C·min^{-1}) then cooled to 100 ºC. A flow of 30 ml·min^{-1} pure NH_3 was passed through the samples for 1 hour, which were then flushed with helium at 100 ºC for 1 hour in order to remove physisorbed NH_3 molecules. NH_3 was thermally desorbed up to 800 ºC with a heating ramp of 10 ºC·min^{-1} and the signal was recorded using a TC (thermal-conductivity) detector.

Thermogravimetric analysis was performed using a Netzsch STA409TP TG/DSC system. A flow of 50 mL·min^{-1} synthetic air was passed through the sample from 25 ºC to 1200 ºC with a heating ramp rate of 10 ºC·min^{-1}.

CNHS elemental analysis on spent catalysts and on the fuel before and after the reaction were performed with a Vario Micro Cube from Elementar.

2.4 Partial dehydrogenation of gasoline E10

Catalyst pellets (diameter of 1.4-1.6 mm; catalyst bed volume of 7 cm^3, average mass of 4 g of catalyst) were placed in the reactor and reduced in a H_2/Ar flow (100 mL·min^{-1}, 4:6 v/v) at 350 ºC and 0.1 MPa for 2 h. The gasoline E10 fuel (8 mL·min^{-1}) was fed to an evaporator that was first preheated for 180 minutes at 380 ºC using a volumetric pump (Shimatzu LC20AD). The temperature of the evaporator was then reduced to 350 ºC. The evaporated fuel was mixed into 29.4 mL·min^{-1} of H_2 (measured at standard conditions of pressure and temperature) to simulate a small recycle of the gas produced and to help avoid coke formation at the surface of the catalyst, and fed to the reactor. The reaction was performed at temperatures of 370 ºC and 400 ºC. At 370

ºC the flow of E10 was 8 mL·min^{-1} and at 400 ºC it was reduced to 7.7 mL·min^{-1} to maintain the same contact time of the reaction. The pressure was 0.8 MPa in the evaporator, the reactor, the condensers and the safety condensers. After the reaction, the gas produced and the evaporated fuel were cooled to room temperature. Two vessels were used to separate the gas phase from the liquid phase at 0.8 MPa and at room temperature. The gas phase was passed through a safety condenser either submerged in water at 20 ºC or in an immersion cooler at -50 ºC, producing hydrogen streams referred to as PDh-1 and PDh-2 respectively. Over the range -70 °C – 20 °C, a temperature of -50 °C was found to be the optimal to separate undesired products (Table S2) from the gas stream. PDh-1 and PDh-2 were analyzed using a gas chromatograph (GC) Agilent 7890A and stored in a 20 L pressure bottle up to 0.7 MPa for later use as the fuel cell feed gas to the anode. The GC was equipped with a dual column system, a HP-PLOT mole sieve 5A column connected to a Thermal Conductivity Detector (TCD) and HP-PLOT/Q column with a Flame Ionization Detector (FID). The TCD was used to detect light gases such as hydrogen, methane or carbon monoxide, while the FID was used for detection of heavier organic compounds such as ethanol, benzene and toluene. A Shimadzu GC 2014 gas chromatograph equipped with a dual column system, a Supel-QTMPLOT column (30 m length × 0.53 mm internal diameter), a fused silica “Y” capillary connector that split the flow to an FID and to second column (DB-17 Agilent J&W, 15 m length × 0.25 mm internal diameter) connected to a flame photometric detector (FPD) was also used to detect sulfur containing compounds in the product gas.

The catalyst recovered after 100 hours of use in the PDh reactor was submitted to two regeneration protocols, a first in 60:40 Ar:H_2 flowed at 100 mL·min^{-1} at 350 °C for 2 hours, and a second in an air flow of 100 mL·min^{-1} at 350 °C for 2 hours, after TGA analysis in air showed that the spent catalyst undergoes a weight loss step at 300 °C.

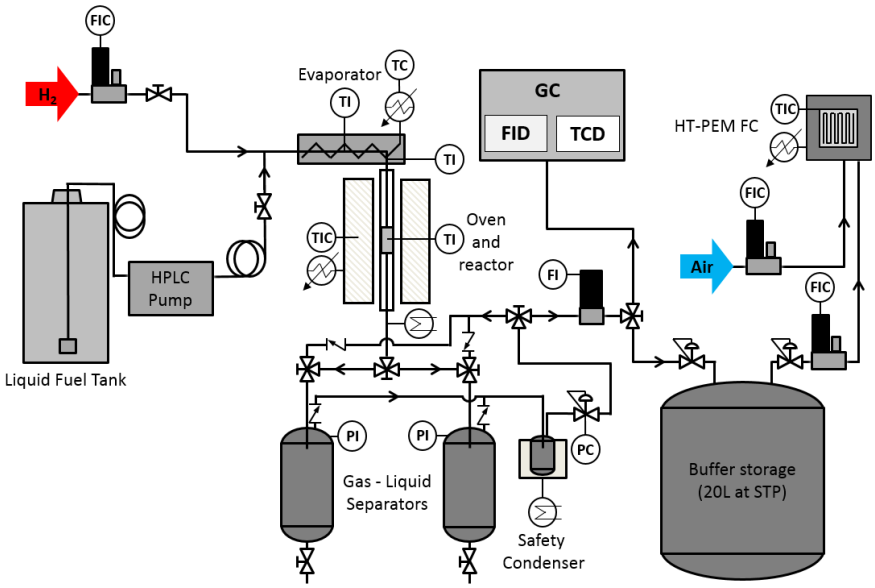

Figure 1. Catalytic partial dehydrogenation test rig coupled with a high temperature proton exchange membrane fuel cell. HPLC (High-Performance Liquid Chromatography pump), FIC (Flow Indicator Controller), FI (Flow Indicator), PI (Pressure Indicator), PC (Pressure Controller), TI (Temperature Indicator), TIC (Temperature Indicator Controller), TC (Temperature Controller), STP (Standard Temperature and Pressure).

The test rig is shown in figure 1. The flow of the gas was measured by a flow indicator and the production rate was calculated using Eq. (1).

$$H_2\ production\ rate = \frac{Produced\ gas\ outflow\ \left(\frac{NL}{h}\right) - Hydrogen\ recycle\ \left(\frac{NL}{h}\right)}{m_{cat}(kg)} \qquad (\mathbf{1})$$

2.5 Characterization of hydrogen-depleted E10 gasoline

The composition of the gasoline recovered following the partial dehydrogenation reaction was determined by elemental analysis. Its density and boiling point were evaluated by using a glass pycnometer and a distillation column, respectively.

2.6 High temperature PEMFC fed with hydrogen produced by partial dehydrogenation of gasoline E10

The gas produced by partial dehydrogenation was used to feed a high temperature single fuel cell equipped with a membrane electrode assembly of active surface area 45 cm^2 type, comprising a phosphoric acid doped polybenzimidazole (PBI) membrane from Advent Technologies. The Advent PBI MEA (Celtec-P1100W) is the successor to the BASF Celtec-P1000 MEA [38]. The test rig used for HT-PEM fuel cell characterization allows the temperature, voltage, current density and pressure to be controlled. First, the fuel cell was heated up to 130 ºC under nitrogen flow at atmospheric pressure. At this temperature, the nitrogen feed was replaced by pure hydrogen at the anode side and synthetic air at the cathode side until 160 ºC was reached. The membrane-electrode assembly was submitted to a break-in procedure at 160 ºC, atmospheric pressure and 200 $mA \cdot cm^{-2}$ for 100 hours with pure hydrogen and synthetic air with a stoichiometry of 4/11.6 respectively, until the cell voltage was stable. Polarization curves were recorded at three different temperatures, 160 ºC, 170 ºC and 190 ºC, using pure hydrogen feed gas. The cell temperature was then lowered to 160 °C, and the polarization measurements repeated using the gas produced by the partial dehydrogenation to feed the anode. The cell temperature was once again lowered to 160 °C and, at an imposed current density of 200 $mA \cdot cm^{-2}$, the cell voltage was measured over a period of 6 hours with an anode/cathode gas stoichiometry of 4/11.6 and, for a further period of 17 hours, with gas stoichiometry 1.8/11.6. The pressure at anode and cathode was atmospheric in all cases. The anode feed was then reverted to pure hydrogen and a polarization curve was recorded at 160 ºC one hour after each constant load hold test, in order to see whether there was any loss in performance of the fuel cell, in that case, a second polarization curve was performed 24 hours after.

3. Results and discussion

3.1 Catalyst characterization

The XRD patterns of the alumina support and the impregnated catalyst are shown in Fig. 2. The diffraction pattern of the support shows peaks characteristic of γ-Al_2O_3, the expected positions of which (ICDD 01-077-0396) are indicated. Following impregnation and calcination, the diffraction peaks characteristic of platinum metal are observed at 39.5º, 46.0º, 67.2º and 81.0º (ICDD 01-087-0646). The platinum crystal size calculated using the Scherrer equation on the diffraction peak at 39.5º provides a coherence length of 8-14 nm. No diffraction lines attributable to tin or indium species are observed, in agreement with earlier work [19]. SEM analysis of the catalyst, Figure S1, shows the structure of the catalyst surface and EDS mapping provided the weight percentage of the active components in the support as being 1.2 % platinum, 1 % tin and 0.6 % indium, in good agreement with the expected values.

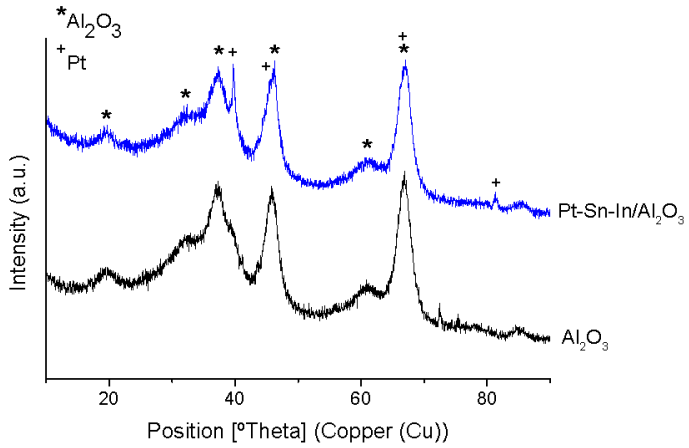

Figure 2. XRD patterns for the ɣ-Al_2O_3 support and Pt-Sn-In/Al_2O_3 catalyst.

The nitrogen adsorption/desorption isotherms and pore diameter distribution of the alumina support and the impregnated catalyst are provided in Fig. 3. Nitrogen adsorption-desorption

isotherms of the alumina support and the In-Pt-Sn/Al_2O_3 catalyst are type IV in the IUPAC classification, characteristic of mesoporous materials, and they present H1-type hysteresis loops, which indicates the presence of cylindrical pore shapes [39]. The surface area of the alumina support calculated using the BET equation is 223 $m^2 \cdot g^{-1}$. It slightly decreases after the co-impregnation and calcination steps to a value of 202 $m^2 \cdot g^{-1}$ for Pt-Sn-In/Al_2O_3. This reduction in specific surface area is accompanied by a decrease in the total pore volume from 0.591 to 0.495 $cm^3 \cdot g^{-1}$, and in the mean pore diameter, calculated using the BJH method, which is centered at 8.4 nm for the support and 7.9 nm for the Pt-Sn-In/Al_2O_3 catalyst.

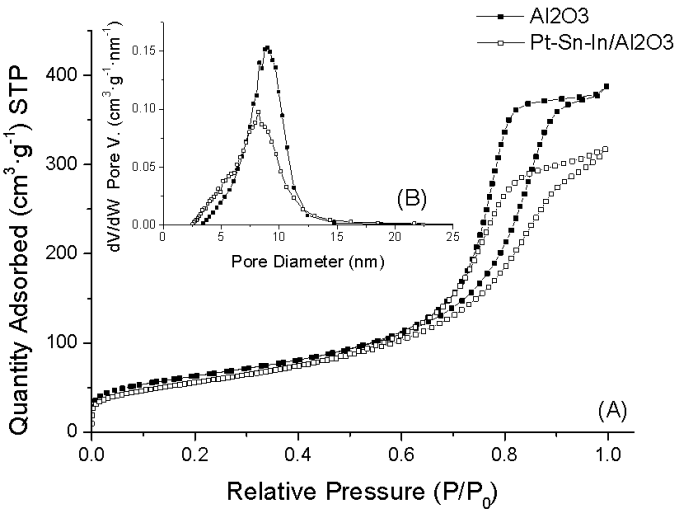

Figure 3. (A) N_2 adsorption (lower curves)-desorption (upper curves) isotherms of ɣ-Al_2O_3 and Pt-Sn-In/ Al_2O_3. (B) Pore size distribution of the ɣ-Al_2O_3 support and Pt-Sn-In/Al_2O_3 catalyst.

The surface acidity of solid acid catalysts can be classified as weak, medium and strong acid sites depending on the temperature at which ammonia is thermally desorbed [40]: weak acid sites when ammonia is desorbed in the range 120-250 ºC, of medium strength between 250 and 350 ºC, and strong acid sites when ammonia is desorbed from 350 to 450 ºC. The surface acidity of the catalyst affects both catalyst activity and selectivity, and also its tendency to cause cracking

and coke formation. Weak acid sites lead to a higher selectivity, whereas strong acid sites of the catalyst can lead to coke formation, which can decrease the activity of the catalyst by masking catalytically active sites [29]. The ammonia-TPD profiles of the alumina support and of the Pt-Sn-In/Al_2O_3 catalyst are plotted in Fig. 4. Analysis of these profiles provides total amount of desorbed ammonia of 354 and 459 $\mu mol_{NH3} \cdot g^{-1}$ for the support and the catalyst respectively.

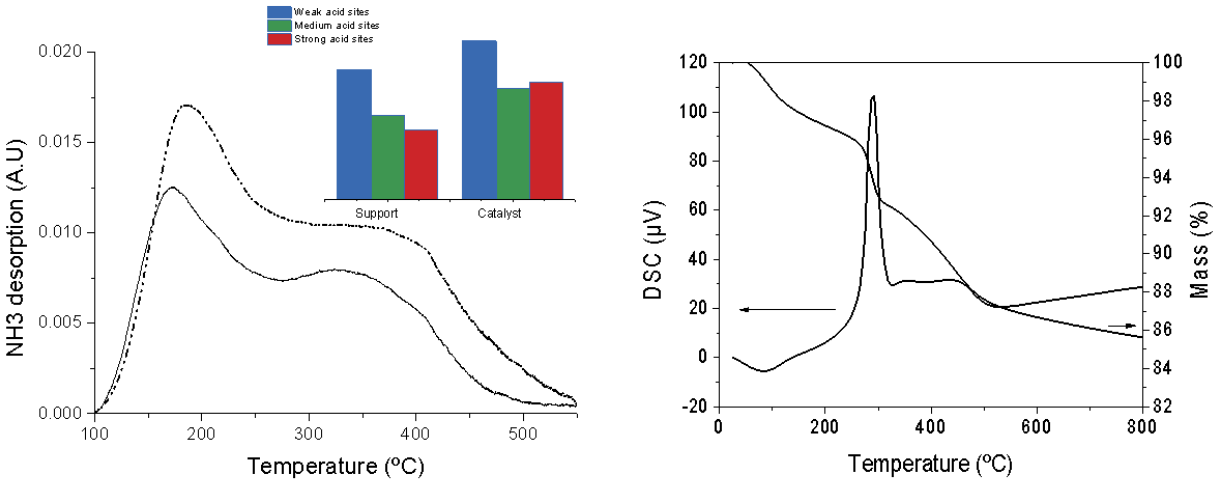

Figure 4. (Left) NH_3-TPD profiles: solid line ɣ-Al_2O_3 support, dashed line Pt-Sn-In/Al_2O_3 catalyst and histogram of the weak, medium and strong acid sites in the support and Pt-Sn-In/Al_2O_3 catalyst. (Right) Thermogravimetric and differential scanning calorimetric analysis of the used catalyst after 100 hours of reaction.

The spent catalyst, after 100 hours of partial dehydrogenation reaction, was analysed using thermogravimetric analysis and the result is presented in Figure 4, right. The catalyst lost 14 % of its weight up to 800 ºC due to the combustion of the carbon coke deposits. Although the weight loss up to 800 °C is continuous, three steps can be identified, and that at 300 °C is accompanied by a strong DSC signal at 292 ºC. This peak can be due to polymerization of ethene produced by ethanol dehydration [17].

A summary of the physicochemical properties of the alumina support and the catalyst after impregnation and calcination is reported in Table 1.

Table 1. Physico-chemical properties of the Al_2O_3 support and the Pt-Sn-In/Al_2O_3 catalyst.

Sample	S_{BET} ($m^2 \cdot g^{-1}$)	D_p (BJH, nm)	V_p ($cm^3 \cdot g^{-1}$)	Surface acidity ($\mu mol_{NH3} \cdot g^{-1}$)
Al_2O_3	223	8.4	0.591	354
Pt-Sn-In/Al_2O_3	202	7.9	0.495	459

The results obtained from elemental analysis of the spent catalyst after 100 hours of reaction are shown in Table 2. The results provide evidence for the deposition of coke, which is likely to be the cause of the deactivation of the catalyst. Indeed, earlier work on partial dehydrogenation of an ethanol-containing gasoline surrogate fuel [17] provided evidence from thermogravimetric-differential thermal analysis for a contribution to the DTA at low temperature (200–250 °C) that was attributed to carbon coke deposited on metal particles via polymerization of ethene formed via ethanol dehydration. The presence of sulfur-containing compounds (or coke) on the catalyst surface provides evidence for desulfurization activity of Pt-Sn-In/Al_2O_3 under the partial dehydrogenation reaction conditions, an outcome that, importantly, reduces the sulfur content of both the depleted gasoline and of the hydrogen gas stream. Carbon and sulfur contents are both significantly removed from the catalyst surface following reductive or oxidative regeneration, Table 2.

Table 2. Elemental analysis of the partial dehydrogenation catalyst before and after 100 hours of partial dehydrogenation reaction and the regenerated catalyst.

	C (%)	H (%)	N (%)	S (%)
Fresh catalyst	0.011	1.428	0	0.002
Spent catalyst after 100 h PDh reaction	6.095	1.330	0	0.118
Catalyst regenerated reductively	4.381	1.090	0.015	0.004
Catalyst regenerated oxidatively	3.137	0.839	0.015	0.014

3.2 Catalytic partial dehydrogenation of E10

Petroleum derivatives such as gasoline and kerosene contain more than 200 different compounds. This makes difficult both their chemical analysis and study of the kinetics of all the possible reactions. Because of this, in previous work, surrogates of gasoline and diesel were used [17]. The commercial fuel of this study is E10, which contains up to 10 % of ethanol, the presence of which can lead to oxygen-containing reaction products including CO and CO_2. Elemental analysis of gasoline E10 provides evidence for the presence also of sulfur and nitrogen containing molecules, the degradation of which during the partial dehydrogenation reaction can potentially give rise to gaseous reaction products as part of the gas stream produced.

The test rig for partial dehydrogenation of E10 contains two gas-liquid separators for separation of the gas phase from the liquid phase. The reaction was carried out at temperatures of 370 ºC and 400 ºC. In a first set of experiments, the reaction was performed at 370 ºC and 400 ºC and the product gas was water-cooled down to room temperature. Figure 5 (a and b) presents the results of the volume of gas produced over 2 hours of reaction. The production rate of the gas at 400 ºC is around 3100 $NL \cdot h^{-1} \cdot kg_{cat}^{-1}$, and around 2700 $NL \cdot h^{-1} \cdot kg_{cat}^{-1}$ at 370 ºC. The purity of the hydrogen at 370 ºC is 94.5±2.1 % and 92.5±2.1 % at 400 ºC. The amount of CO increases from 0.7±0.2 % at 370 ºC to 1.4±0.2 % at 400 ºC. No hydrogen sulfide was detected. Over a set time

interval, although the volume of product gas is higher for reaction at 400 ºC, the CO content is also higher, and thus a reaction temperature of 370 °C was chosen for further optimization of reaction conditions. The catalyst recovered after regeneration was used in these conditions to evaluate the efficacy of the regeneration protocol, when the initial productivity was found fully comparable to the above results obtained with the fresh catalyst in the first 4 hours : 2680 $NL \cdot h^{-1} \cdot kg_{cat}^{-1}$ (regenerated catalyst) ; 2690 $NL \cdot h^{-1} \cdot kg_{cat}^{-1}$ (fresh catalyst).

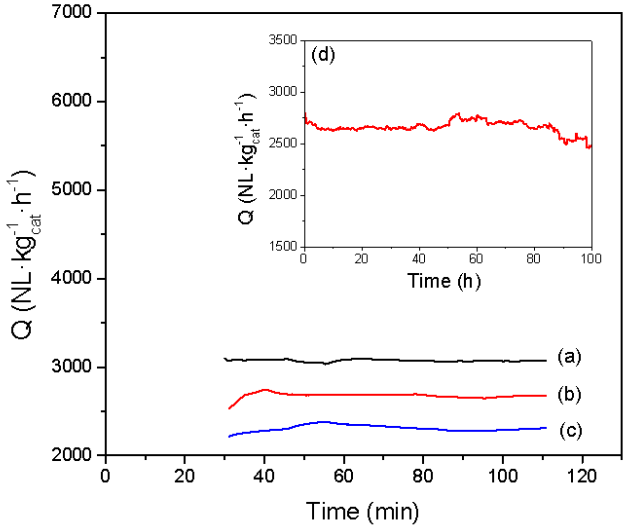

Figure 5. Gas production by the partial dehydrogenation reaction of E10. Influence of the reactor temperature (a) 400 ºC (b, c, d) 370 ºC. The product gas was flowed through a condenser at room temperature in (a, b and d) and at -50 °C in (c).

A liquid nitrogen cold trap can be used to trap impurities [41] from the gas stream produced. In the present work, in a second set of experiments the condenser was cooled to -50 ºC using an immersion cooler IP-60 with a rigid coil probe to cold-trap the light organic compounds from the gas phase and thereby increase the purity of the hydrogen stream. In this case the productivity is lower, around 2300 $NL \cdot h^{-1} \cdot kg_{cat}^{-1}$, but the purity of the hydrogen is significantly

higher, 98.6±2.1 % due to the removal of organic components. The hydrogen productivity with time at a reaction temperature of 370 °C with a condensation-separation step at 20 °C or at -50 °C is presented in Figure 5 (b and c), and the corresponding gas compositions (PDh-1 and PDh-2 respectively) are provided in Table 3. Both the specific rate of hydrogen production and the purity are notably higher than those obtained in our earlier work on partial dehydrogenation of a gasoline surrogate containing ethanol (900 $NL \cdot h^{-1} \cdot kg_{cat}^{-1}$; hydrogen purity of 70 %). The differences found in the productivity and hydrogen purity are due to a combination of factors including the reaction conditions, which were not completely optimized (0.1 MPa, 350 ºC and 2 seconds of contact time without hydrogen recycle), catalyst properties and the composition of the surrogate that comprised 13.5 % n-heptane, 37.5 % iso-octane, 9 % cyclohexane, 6 % cyclohexene, 30.5 % toluene and 3.5 % ethanol [17].

Table 3. Gas composition from partial dehydrogenation of E10 gasoline at 370 °C after either water-cooling to room temperature (PDh-1, PDh-3) or passing through a cold-trap at -50 °C (PDh-2). PDh-1 and PDh-2 were produced using fresh catalysts; PDh-3 using a regenerated catalyst.

PDh product	Gas production ($NL \cdot h^{-1} \cdot kg_{cat}^{-1}$)	Condenser temperature (°C)	H_2 (%)	CH_4 (%)	N_2 (%)	CO (%)	Organic Compounds (%)
PDh-1	2700	20	94.5	0.4	0.3	0.7	4.1
PDh-2	2300	-50	98.6	0.4	0.3	0.7	0
PDh-3	2680	20	94.2	0.7	0.3	1.0	3.8

A longer-term PDh reaction was performed over a total duration of 100 hours, to prove the feasibility of a system for hydrogen delivery, including start and stop procedures. The long-term reaction was carried out discontinuously, with 5 hours reaction each day, following which the

reaction was stopped, the reactor cooled down to room temperature and the reaction started up and continued the next day. Fig. 5d presents the hydrogen productivity over 100 hours. The average hydrogen production from gasoline E10 over this period is 2700 $NL \cdot h^{-1} \cdot kg_{cat}^{-1}$ with a decay rate of 3.8 $NL \cdot h^{-1} \cdot kg_{cat}^{-1}$. The hydrogen produced after 100 hours is around 94 % pure, with the amount of CO having increased from 0.7 to 1.3 % over time. The gases produced by partial dehydrogenation of SP95E10 with a separation step at 20 °C (PDh-1) and at -50 ºC (PDh-2), Table 3, were stored in 20 L gas cylinders at 0.7 MPa before use as the anode gas for HT-PEMFC. In earlier work, the catalyst was considered to be deactivated when hydrogen production reached 1500 $NL \cdot h^{-1} \cdot kg_{cat}^{-1}$. In the present work, the catalyst lifetime estimated by linear extrapolation of the hydrogen productivity to 1500 $NL \cdot h^{-1} \cdot kg_{cat}^{-1}$ corresponds to 2140 h (83 days).

A benefit of partial dehydrogenation is that the fuel composition should remain largely unchanged, and still correspond in its macroscopic properties to the initial fuel, meaning that it is still suitable for use in a combustion engine. The composition of the depleted (partially dehydrogenated) fuel is presented in Table 4, which indicates that the reaction has led to a reduction in the heteroatom content (N, O, S) and, correspondingly, increased carbon and hydrogen content. While the decomposition of ethanol probably accounts in part for the decrease in oxygen content, the initial composition of gasoline is too complex to suggest reaction pathways for nitrogen and sulfur containing components. It is important to note that no gaseous sulfur components were detected in the product gas, the sulfur balance probably being provided by the sulfur deposited with carbon coke on the catalyst surface (Table 2). In contrast, nitrogen was not detected on the spent catalyst and yet is of lower content in the gasoline after reaction than before reaction. This suggests that one more or more nitrogen compounds, in addition to N_2, might be present in the gas stream produced by partial dehydrogenation.

Table 4. Elemental analysis of the gasoline E10 before and after partial dehydrogenation.

	C (%)	H (%)	N (%)	S (%)	O (%)
E10 before	83.465	10.968	2.702	0.034	2.660
E10 after	85.969	11.658	1.250	0.003	1.12

3.3 High temperature PEMFC operation with hydrogen produced by partial dehydrogenation of gasoline E10

Polarization curves (iV curves) were first recorded using pure hydrogen (99.995 %) at the anode at three different temperatures, and then the feed gas stream was switched to PDh-1 (Table 3).

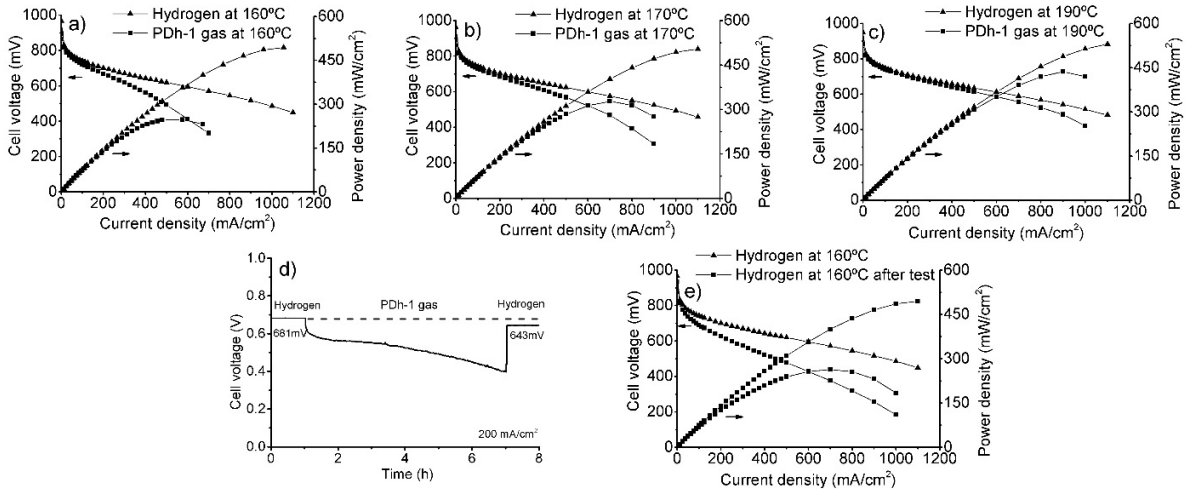

Figure 6. a) IV-curves and corresponding power density plots at 160 ºC for an HT-PEMFC fed with pure hydrogen and PDh-1 gas. b) IV-curves at 170 ºC of pure hydrogen and PDh-1 gas. c) IV-curves at 190 ºC of pure hydrogen and PDh-1 gas. d) Cell voltage vs. time at 200 mA·cm^{-2}

and 160 ºC using PDh-1 gas at the anode. e) IV-curves on pure hydrogen before and after the current density hold test at 160 ºC.

The purpose of the research described here is to compare the performance of the high temperature PEMFC when operated with pure hydrogen and with the gas produced by PDh, however comparison of the results obtained with Celtec P1100W MEAs with previously reported results is also important. The polarization curves obtained with H_2-air at 160, 170 and 190 °C are provided in Figure 6(a-c); a potential of 0.595 V measured at the current density of 600 $mA \cdot cm^{-2}$ is in full agreement with results reported earlier [42]. The fuel cell performance increases with cell temperature, as expected, with both H_2 and PDh-1. Although the cell voltage at current densities above 50 $mA \cdot cm^{-2}$ is significantly lower at all temperatures when PDh-1 is used than pure H_2, this voltage loss is highest at 160 °C and it becomes progressively lower at higher temperature. This observation suggests that at 160 °C the use of PDh-1 leads to partial poisoning of catalytic sites for hydrogen oxidation at the anode and that the adsorbed species are at least partially removed at 190 °C.

Some gaseous compounds produced by the PDh reforming, such as nitrogen or methane, are considered as causing dilution of the hydrogen stream but do not poison the catalyst active sites and are without impact on the fuel cell performance. In contrast, compounds possibly formed during the PDh reaction such as carbon monoxide, ammonia or other nitrogen containing compounds, or hydrogen sulfide, can interact with the platinum surface, blocking active sites and preventing the adsorption of hydrogen, which leads to a loss of the performance [43–48]. In general, HT-PEMFC operating at 160 °C tolerates a concentration of up to 3 % CO, higher CO concentrations leading to greater loss of cell voltage. The adsorption of CO on the platinum catalyst surface is an exothermic reaction and can be decreased by increasing the operation

temperature [49]. The chemical analysis results of Table 3 indicate that the sulfur content of the initial E10 gasoline used in the PDh reaction (0.034 % sulfur), was reduced by an order of magnitude by the PDh reaction to a residual 30 ppm of sulfur in the depleted gasoline. This suggests that either the exit stream of the PDh gas comprises a sulfur containing component (and, indeed, conventional reforming of gasoline produces hydrogen sulfide [37]) or that the sulfur was removed as a solid residue on the spent catalyst. In the present case, indeed no H_2S was detected by gas chromatography using an FPD detector, and elemental analysis of the used catalyst showed the presence of 0.119 % sulfur on the catalyst surface. Similarly, the nitrogen content of the depleted gasoline decreased from 2.70 to 1.26 %, but the elemental analysis of the used catalyst showed no nitrogen, inferring that the PDh-1 gas comprises nitrogen containing components. Like carbon monoxide, H_2S and NH_3 also bind to platinum [50] causing a strong loss in fuel cell performance, but in this case the initial performance cannot be recovered. However, neither NH_3 nor H_2S were detected in the PDh-1 gas, which suggests that one or more of the organic product components contains nitrogen (and possibly sulfur). It may be concluded that the voltage loss of the HT-PEMFC when using PDh-1 comprises recoverable and irrecoverable components corresponding to adsorption/desorption of CO and to nitrogen (and possibly sulfur) containing organic compounds respectively.

The voltage loss with time of the fuel cell fed with the gas produced by partial dehydrogenation of gasoline was monitored by imposing a current density of 200 $mA \cdot cm^{-2}$ with PDh-1 gas fed to the HT-PEM fuel cell. The cell voltage decreased rapidly over the 6 hours of the current density hold, from 681 mV to 396 mV, which corresponds to an average degradation rate of -30 $mV \cdot h^{-1}$ (figure 6d). The anode gas stream was then switched to pure hydrogen for a further seven days when the HT-PEMFC underwent rapid, although incomplete recovery, to 643 mV at 200 $mA \cdot cm^{-2}$, i.e. to 93 % of the initial cell voltage. The loss in performance of the fuel cell may also be seen

in the polarization curve recorded after the test (figure 6e), without detecting any significant change in it due to the irreversible poisoning of catalytic sites.

A fresh Celtec P1100W MEA was used when the gas stream PDh-2 was fed to the fuel cell and polarization curves recorded at 160, 170 and 190 °C. The results are presented in Figure 7(a-c). In this case the voltage drop from that obtained with pure hydrogen is lower in each case than observed when using PDh-1 gas to feed the fuel cell and, when the temperature was increased to 190 °C, the performance is comparable with that obtained with pure hydrogen. At 160 ºC and current density of 200 $mA \cdot cm^{-2}$, the cell voltage dropped from 679 mV to 667 mV, i.e. -0.3 $mV \cdot h^{-1}$, 100 times lower than observed when using PDh-1 anode gas. Further, this loss is fully recovered on switching back to pure hydrogen (figure 7d) and a polarization curve (figure 7e) recorded at this point is identical to that determined initially. It may be concluded that the introduction of a low temperature trap in the process used to prepare PDh gas is of crucial importance in producing a hydrogen stream by partial dehydrogenation of gasoline free from heteroatom substituted organic compounds that is directly usable by a high temperature PEMFC.

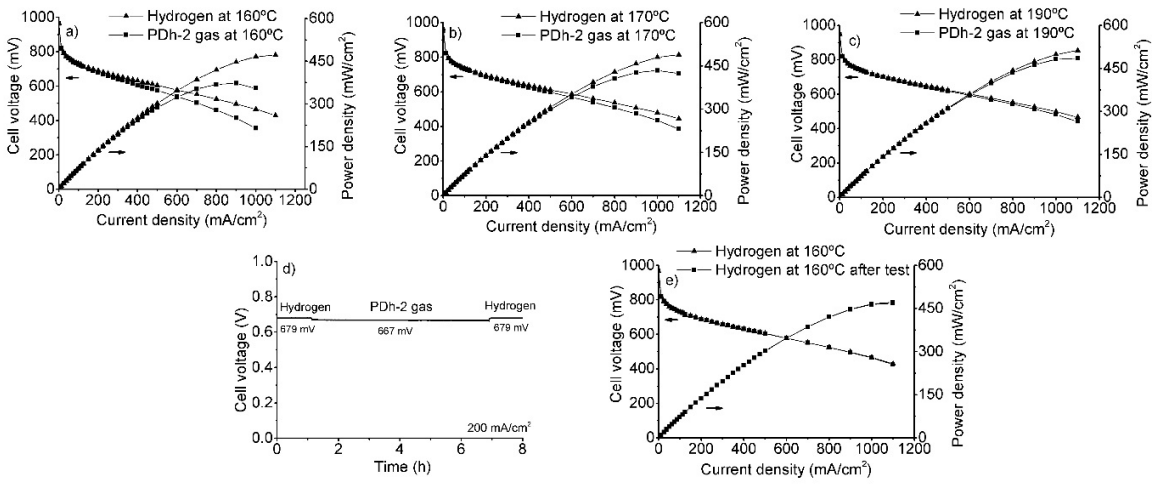

Figure 7. a) IV-curves and corresponding power density plots at 160 ºC for an HT-PEMFC fed with pure hydrogen and PDh-2 gas. b) IV-curves at 170 ºC of pure hydrogen and PDh-2 gas. c)

IV-curves at 190 ºC of pure hydrogen and PDh-2 gas. d) Cell voltage vs. time at 200 mA·cm^{-2} and 160 ºC using PDh-2 gas at the anode. e) IV-curves on pure hydrogen before and after the current density hold test at 160 ºC.

Using a lower anode stoichiometry of 1.8 enabled longer duration hold using the prepared 20 L cylinder of PDh-2 gas (17 hours) at 200 mA·cm^{-2}. The voltage loss of 0.8 mV·h^{-1} (figure 8a), is slightly higher than in the results of Figure 7d, but once again the initial cell voltage was completely recovered when pure hydrogen was fed, and the initial and final polarization curves under pure hydrogen, after 17 hours of operation with PDh-2 gas, are identical (figure 8b).

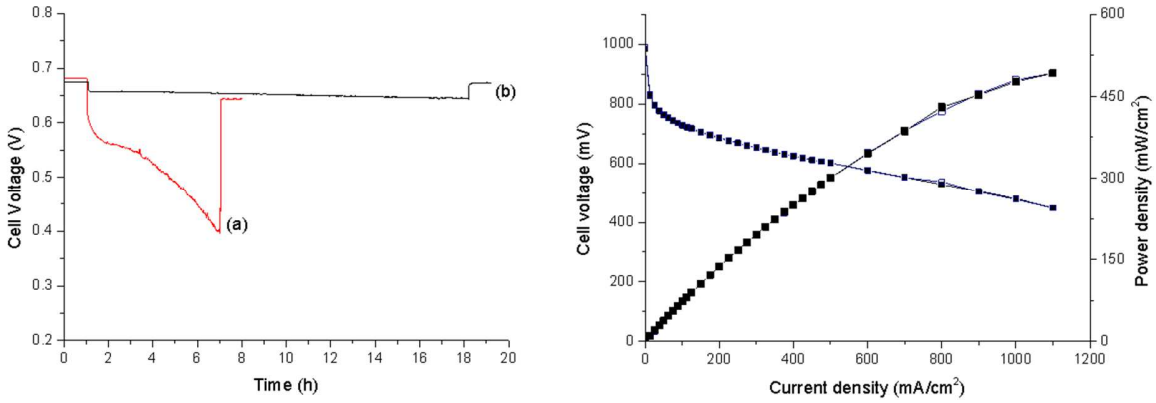

Figure 8. (Left) Current density hold at 200 mA·cm^{-2} and 160 ºC (a) with PDh-1 and (b) PDh-2 gas fed to the high temperature PEMFC. (Right) Polarization curves and corresponding power density plot at 160 °C obtained with pure hydrogen (■) before and (□) after operation for 17 hours with PDh-2.

4. Conclusions

The partial dehydrogenation of E10 gasoline leads to production of hydrogen from a combustible liquid fuel with a productivity of up to 2700 $NL \cdot h^{-1} \cdot kg_{cat}^{-1}$. The depleted gasoline retains a density of 742 $kg \cdot m^{-3}$ and boiling point of 204 ºC within the industry specifications, 720-775 $kg \cdot m^{-3}$ and 190-210 ºC [34], meaning that it can be recycled into the fuel tank for use in a combustion engine. Importantly, the PDh reaction also has a significant desulfurization effect, since the sulfur content of depleted gasoline is only one-tenth of its initial value. Using an optimised catalyst test rig incorporating a low temperature condenser to trap organic side-products of the PDh reaction, the purity of the hydrogen reaches 98.6 %, the remaining 1.4 % comprising CO, CH_4 and N_2 with an average production of 2300 $NL \cdot h^{-1} \cdot kg_{cat}^{-1}$. This PDh gas can be directly used as anode feed gas to a high temperature PEMFC without any additional purification step. This is the first time that PDh hydrogen from gasoline has been coupled to a fuel cell, and both the production of hydrogen and its use in the fuel cell seen to present low degradation rates, while also providing evidence that the properties of the liquid hydrogen-carrier fuel (E10 gasoline) are sufficiently unchanged to allow its original use.

Acknowledgement

RGG gratefully acknowledges the financial support of Région Occitanie, Safran S.A. and EIFER - European Institute for Energy Research for a personal research fellowship. The authors acknowledge Calypso Baril from the Microscopie Electronique et Analytique platform, Université de Montpellier, for the SEM observations and corresponding sample preparation.

References

[1] R. Can, J. Pasel, R. Peters, D. Stolten, Fuel cell systems with reforming of petroleum-based and synthetic-based diesel and kerosene fuels for APU applications, Int. J. Hydrogen

Energy. 40 (2015) 6405–6421.

[2] B. Tanc, H. Turan Arat, E. Baltacioglu, K. Aydin, Overview of the next quarter century vision of hydrogen fuel cell electric vehicles, Int. J. Hydrogen Energy. 44 (2019) 10120–10128.

[3] Y. Hames, K. Kaya, E. Baltacioglu, A. Turksoy, Analysis of the control strategies for fuel saving in the hydrogen fuel cell vehicles, Int. J. Hydrogen Energy. 43 (2018) 10810–10821.

[4] D. Mori, K. Hirose, Recent challenges of hydrogen storage technologies for fuel cell vehicles, Int. J. Hydrogen Energy. 34 (2009) 4569–4574.

[5] J. Martin, P. Millington, B. Campbell, L. Barron, S. Fisher, On-board generation of hydrogen to improve in-cylinder combustion and after-treatment efficiency and emissions performance of a hybrid hydrogen-gasoline engine, Int. J. Hydrogen Energy. 44 (2018) 12880–12889.

[6] L.A. Tuan, N.T. Luong, K.N. Ishihara, Ni-Cu/Al_2O_3 catalysts for gasoline reforming to produce hydrogen applied in spark ignition engines, Catalysts. 6 (2016) 45.

[7] C. Fabiano, C. Italiano, A. Vita, L. Pino, M. Lagana, V. Recupero, Performance of 1.5 Nm^3/h hydrogen generator by steam reforming of n-dodecane for naval applications, 41 (2016) 19475–19483.

[8] R.C. Samsun, D. Krekel, J. Pasel, M. Prawitz, R. Peters, A diesel fuel processor for fuel-cell-based auxiliary power unit applications, J. Power Sources. 355 (2017) 44–52.

[9] R.C. Samsun, M. Prawitz, A. Tschauder, J. Pasel, R. Peters, D. Stolten, An autothermal reforming system for diesel and jet fuel with quick start-up capability, Int. J. Hydrogen Energy. 44 (2019) 27749–27764.

[10] P. Ribeirinha, I. Alves, V.F. Vazquez, G. Schuller, M. Boaventura, A. Mendes, Heat

integration of methanol steam reformer with a high-temperature polymeric electrolyte membrane fuel cell, Energy. 120 (2017) 468–477.

[11] S. Zhang, Y. Zhang, J. Chen, C. Yin, X. Liu, Design , fabrication and performance evaluation of an integrated reformed methanol fuel cell for portable use, J. Power Sources. 389 (2018) 37–49.

[12] C. Pan, R. He, Q. Li, J.O. Jensen, N.J. Bjerrum, H.A. Hjulmand, A.B. Jensen, Integration of high temperature PEM fuel cells with a methanol reformer, J. Power Sources. 145 (2005) 392–398.

[13] W. Waiblinger, S. Auvinen, P. Ribeirinha, Heat and fuel coupled operation of a high temperature polymer electrolyte fuel cell with a heat exchanger methanol steam reformer, J. Power Sources. 347 (2017) 47–56.

[14] C. Diehm, T. Kaltschmitt, O. Deutschmann, Hydrogen production by partial oxidation of ethanol/gasoline blends over Rh/Al_2O_3, Catal. Today. 197 (2012) 90–100.

[15] D. Teichmann, W. Arlt, P. Wasserscheid, R. Freymann, A future energy supply based on Liquid Organic Hydrogen Carriers (LOHC), Energy Environ. Sci. 4 (2011) 2767–2773.

[16] E. Gianotti, M. Taillades-Jacquin, J. Roziere, D.J. Jones, High-Purity Hydrogen Generation via Dehydrogenation of Organic Carriers : A Review on the Catalytic Process, ACS Catal. 8 (2018) 4660–4680.

[17] E. Gianotti, M. Taillades-Jacquin, Á. Reyes-Carmona, G. Taillades, J. Rozière, D.J. Jones, Hydrogen generation via catalytic partial dehydrogenation of gasoline and diesel fuels, Appl. Catal. B, Environ. 185 (2016) 233–241.

[18] E. Gianotti, Á. Reyes-Carmona, K. Pearson, M. Taillades-Jacquin, G. Kraaij, A. Wörner, J. Rozière, D.J. Jones, Hydrogen generation by catalytic partial dehydrogenation of low-sulfur fractions produced from kerosene Jet A-1, Appl. Catal. B, Environ. 176–177 (2015)

480–485.

[19] E. Gianotti, Á. Reyes-Carmona, M. Taillades-Jacquin, G. Taillades, J. Rozière, D.J. Jones, Study of the effect of addition of In to Pt-Sn / γ-Al_2O_3 catalysts for high purity hydrogen production via partial dehydrogenation of kerosene jet A-1, Appl. Catal. B, Environ. 160–161 (2014) 574–581.

[20] M. Taillades-Jacquin, C. Resini, K. Liew, G. Taillades, I. Gabellini, D. Wails, J. Rozière, D. Jones, Environmental Effect of the nature of the support on the activity of Pt-Sn based catalysts for hydrogen production by dehydrogenation of Ultra Low Sulfur Kerosene Jet A-1, Appl. Catal. B, Environ. 142–143 (2013) 112–118.

[21] Á. Reyes-Carmona, E. Gianotti, M. Taillades-Jacquin, G. Taillades, J. Rozière, E. Rodríguez-Castellón, D.J. Jones, High purity hydrogen from catalytic partial dehydrogenation of kerosene using saccharide-templated mesoporous alumina supported Pt-Sn, Catal. Today. 210 (2013) 26–32.

[22] C. Lucarelli, S. Albonetti, A. Vaccari, C. Resini, G. Taillades, J. Roziere, K.E. Liew, A. Ohnesorge, C. Wolff, I. Gabellini, D. Wails, On-board H_2 generation by catalytic dehydrogenation of hydrocarbon mixtures or fuels, Catal. Today. 175 (2011) 504–508.

[23] C. Resini, C. Lucarelli, M. Taillades-Jacquin, K.-E. Liew, I. Gabellini, S. Albonetti, D. Wails, J. Roziere, A. Vaccari, D. Jones, Pt–Sn γ-Al_2O_3 and Pt–Sn–Na γ-Al_2O_3 catalysts for hydrogen production by dehydrogenation of Jet A-1 fuel Characterisation and preliminary activity tests, Int. J. Hydrogen Energy. 36 (2011) 5972–5982.

[24] M.R. Rahimpour, M. Jafari, D. Iranshahi, Progress in catalytic naphtha reforming process: A review, Appl. Energy. 109 (2013) 79–93.

[25] J. Lee, E.J. Jang, J.H. Kwak, Effect of number and properties of specific sites on alumina surfaces for Pt-Al_2O_3 catalysts, Appl. Catal. A Gen. 569 (2019) 8–19.

[26] O.O. James, S. Mandal, N. Alele, B. Chowdhury, S. Maity, Lower alkanes dehydrogenation : Strategies and reaction routes to corresponding alkenes, Fuel Process. Technol. 149 (2016) 239–255.

[27] S.A. Bocanegra, A.A. Castro, O.A. Scelza, S.R. de Miguel, Characterization and catalytic behavior in the n-butane dehydrogenation of trimetallic InPtSn/$MgAl_2O_4$ catalysts, Appl. Catal. A Gen. 333 (2007) 49–56.

[28] S.A. Bocanegra, A. Guerrero-Ruiz, S.R. de Miguel, O.A. Scelza, Performance of PtSn catalysts supported on MAl_2O_4 (M: Mg or Zn) in n-butane dehydrogenation: Characterization of the metallic phase, Appl. Catal. A Gen. 277 (2004) 11–22.

[29] S. He, C. Sun, Z. Bai, X. Dai, B. Wang, Dehydrogenation of long chain paraffins over supported Pt-Sn-K/Al_2O_3 catalysts: A study of the alumina support effect, Appl. Catal. A Gen. 356 (2009) 88–98.

[30] S. He, W. Bi, Y. Lai, X. Rong, X. Yang, C. Sun, Effect of Sn promoter on the performance of Pt-Sn/γ-Al_2O_3 catalysts for n-dodecane dehydrogenation, J. Fuel Chem. Technol. 38 (2010) 452–457.

[31] X. Liu, W.Z. Lang, L.L. Long, C.L. Hu, L.F. Chu, Y.J. Guo, Improved catalytic performance in propane dehydrogenation of PtSn/γ-Al_2O_3 catalysts by doping indium, Chem. Eng. J. 247 (2014) 183–192.

[32] S. Albonetti, E. Boanini, I. Jiménez-Morales, C. Lucarelli, M. Mella, C. Molinari, A. Vaccari, Novel thiotolerant catalysts for the on-board partial dehydrogenation of jet fuels, RSC Adv. 6 (2016) 48962–48972.

[33] The European Renewable Ethanol Association, An ethanol blend to fuel Europe's clean mobility, https://epure.org/media/1886/190509-def-pr-revised-epure-e10-leaflet_en_web.pdf. (accessed December 11, 2020).

[34] Total, Total super premier 95-E10 Fiche de caractéristiques, https://www.total.fr/sites/shared/msfrance/files/atoms/files/fiche-technique-total-super-premier-95-e10.pdf. (accessed December 10, 2020).

[35] T.J. Schmidt, J. Baurmeister, Properties of high-temperature PEFC Celtec-P 1000 MEAs in start/stop operation mode, J. Power Sources. 176 (2008) 428–434.

[36] A. Bulgarin, H. Jorschick, P. Preuster, A. Bosmann, P. Wasserscheid, Purity of hydrogen released from the Liquid Organic Hydrogen Carrier compound perhydro dibenzyltoluene by catalytic dehydrogenation, Int. J. Hydrogen Energy. 45 (2020) 712–720.

[37] F. Valle, Electrocatalyst degradation in high temperature PEM fuel cells, University of Trieste, 2014.

[38] V. Gurau, E. S. De Castro, Prediction of performance variation caused by manufacturing tolerances and defects in gas diffusion electrodes of phosphoric acid (PA)– Doped polybenzimidazole (PBI)-Based High-Temperature proton exchange membrane fuel cells, Energies. 13 (2020) 1–14.

[39] S.J. Gregg, K.S.W. Sing, Adsorption, Surface Area and Porosity, Second Edi, 1982.

[40] S. Narayanan, A. Sultana, Q. Thinh, A. Auroux, A comparative and multitechnical approach to the acid character of templated and non-templated ZSM-5 zeolites, 168 (1998) 373–384.

[41] K.-E. Liew, Fondements de la déshydrogenation partielle: étude théorique et expérimentale sur un nouveau combustible méthode de traitment pour générer de l´hydrogéne à partir de jet fuel, Université de Montpellier, 2011.

[42] M.G. Waller, M.R. Walluk, T.A. Trabold, Performance of high temperature PEM fuel cell materials . Part 1 : Effects of temperature , pressure and anode dilution, Int. J. Hydrogen Energy. 41 (2016) 2944–2954.

[43] P. Mocotéguy, B. Ludwig, J. Scholta, Y. Nedellec, D.J. Jones, J. Rozière, Long-term testing in dynamic mode of HT-PEMFC H_3PO_4/PBI celtec-P based membrane electrode assemblies for micro-CHP applications, Fuel Cells. 10 (2010) 299–311.

[44] S.J. Andreasen, J.R. Vang, S.K. Kær, High temperature PEM fuel cell performance characterisation with CO and CO_2 using electrochemical impedance spectroscopy, Int. J. Hydrogen Energy. 36 (2011) 9815–9830.

[45] V.A. Sethuraman, L. Wise, S. Balasubramanian, J.W. Weidner, Hydrogen Sulfide Kinetics on PEM Fuel Cell Electrodes, ECS Trans. 1 (2006) 111–130.

[46] M. Rau, C. Cremers, J. Tübke, Development of anodic materials for HT-PEMFCs with high tolerance to H_2S, Int. J. Hydrogen Energy. 40 (2015) 5439–5443.

[47] J.B. Thomas J. Schmidt, Durability and reliability in high-temperature reformed hydrogen PEFCs, Electrochem. Sciety. 3 (2006) 861–869.

[48] A. Dushina, D. Schonvogel, Y. Fischer, J. Büsselmann, A. Dyck, P. Wagner, Influence of Ammonia Contamination on HT-PEM fuel cell platinum catalyst, ECS Trans. 98 (2020) 537.

[49] B. Shabani, M. Hafttananian, S. Khamani, A. Ramiar, A.A. Ranjbar, Poisoning of proton exchange membrane fuel cells by contaminants and impurities : Review of mechanisms , effects , and mitigation strategies, J. Power Sources. 427 (2019) 21–48.

[50] V.A. Sethuraman, J.W. Weidner, Analysis of Sulfur Poisoning on a PEM Fuel Cell Electrode, 55 (2010) 5683–5694.